Journal of Theoretical Biology 485 (2020) 110042

Contents lists available at ScienceDirect

Journal of Theoretical Biology

journal homepage: www.elsevier.com/locate/jtb

Cross-inhibition of Turing patterns explains the self-organized regulatory mechanism of planarian fission

Samantha Herath[a], Daniel Lobo[a,b,*]

[a] Department of Biological Sciences, University of Maryland, Baltimore County, 1000 Hilltop Circle, Baltimore, MD 21250, United States
[b] Department of Computer Science and Electrical Engineering, University of Maryland, Baltimore County, 1000 Hilltop Circle, Baltimore, MD 21250, United States

ARTICLE INFO

Article history:
Received 2 April 2019
Revised 24 September 2019
Accepted 10 October 2019
Available online 12 October 2019

Keywords:
Regeneration
Fission
Planaria
Turing
Reaction-diffusion
Patterning
Asexual reproduction

ABSTRACT

Planarian worms reproduce asexually by fission, resulting in two separated pieces each repatterning and regenerating a complete animal. The induction of this process is known to be dependent on the size of the worm as well as on environmental factors such as population density, temperature, and light intensity. However, despite much progress in understanding the signaling mechanisms of planarian regeneration and the biomechanics of fissioning, no induction mechanism has been proposed for the signaling of fission. Here, we propose and analyze a cross-inhibited Turing system in a growing domain for the signaling of fission in planaria and the regeneration of the anterior-posterior opposite head and tail gene expression gradient patterns. This self-regulated mechanism explains when and where growing planaria fission, and its dependence on the worm length. Furthermore, we show how a delayed control mechanism of the cross-inhibited Turing system explains the asymmetry of the resulting fragments, the induction of fission with an anterior amputation even in a short worm, the consecutive multiple fissions called fragmentation, and the effects of environmental factors in the signaling of fission. We discuss the possible molecular and biophysical implementations of the proposed model and suggest specific experiments to elucidate them. In summary, the proposed controlled cross-inhibited Turing system represents a completely self-regulated model of the fission and regeneration signaling in planaria.

1. Introduction

Planarians have the capability to repattern and regenerate their complete bodies, including their complex organs, from almost any amputation (Lobo et al., 2012; Cebrià et al., 2018; Forsthoefel and Newmark, 2009; Reddien and Sánchez Alvarado, 2004). This extraordinary regenerative capacity lets them reproduce asexually by fissioning their bodies through a plane normal to the anterior-posterior axis, which results in two separated worm pieces each regenerating a complete new worm (Best et al., 1969; Yang et al., 2017). The execution of fission can be explained through biomechanics including local constriction, pulsation and transverse rupture, yet the induction signaling molecular mechanism controlling when and where the worms fission remains unknown (Malinowski et al., 2017).

Fission in planaria can be affected by several internal and external factors. One of the primary factors that induces fission is worm length. In a 4-day span experiment, isolated *Dugesia dorotocephala* planarian flatworms of short lengths (6 to 8 mm) do not fission, 15% of medium worms (10 to 12 mm) fission, and 40% of long worms (15 to 17 mm) fission (Best et al., 1969). Similarly, the area size of *Schmidtea mediterranea* planarian flatworms positively correlates with the probability of fission (Thomas et al., 2012; Quinodoz et al., 2011), and worms shorter than 4–5 mm do not fission (Arnold et al., 2019). *Dugesia japonica* fission only after reaching a body length of 8 mm (Sakurai et al., 2012), while *Girardia tigrina* fission probability depends on the previous fissions—a generational memory effect—in addition to its size (Yang et al., 2017). Amputation of anterior areas increases the fission probability in planaria (Best et al., 1969; Malinowski et al., 2017; Child, 1910), which suggests that the anterior region produces inhibitory signals that prevent fission (Newmark and Alvarado, 2002; Brøndsted, 1969). Although the posterior fragments in flatworms rarely fission further until regeneration is complete and the worm grows longer (Best et al., 1975), the anterior fragments can undergo multiple consecutive divisions within a short time span (Quinodoz et al., 2011; Best et al., 1975) along vulnerable planes along the anterior-posterior axis (Arnold et al., 2019), a process referred to as fragmentation (Thomas et al., 2012). Importantly, the Wnt and TGFβ signaling pathways have been shown to participate

* Corresponding author at: Department of Biological Sciences, University of Maryland, Baltimore County, 1000 Hilltop Circle, Baltimore, MD 21250, United States
E-mail address: lobo@umbc.edu (D. Lobo).

https://doi.org/10.1016/j.jtbi.2019.110042
0022-5193/

in fission signaling: RNA interference (RNAi) of *β-catenin, actR-1, smad2/3,* and *wnt11-6* reduces fission frequency, whereas RNAi of *apc* increases fission frequency (Arnold et al., 2019). Additionally, environmental factors can affect the fission probability at a given length. Higher population density increases social physical interaction, which can inhibit the fission signaling (Best et al., 1975; Best et al., 1974; Pigon et al., 1974). Conversely, higher temperatures shorten the length at which planarians fission (Handberg-Thorsager and Saló, 2007), in the same way than darker environments (Morita and Best, 1984; Sheĭman et al., 2003). Despite this comprehensive experimental knowledge of the fission behavior in planaria, no mechanistic explanation has been proposed for the signaling of fission or fragmentation.

Although no model exists for planarian fission, the pattern and regeneration of the planarian head and tail signals can be explained by models based on Turing self-organizing systems of pattern formation (Turing, 1952) and its later developments as reaction-diffusions systems (Gierer and Meinhardt, 1972; Meinhardt and Gierer, 1974). The molecular basis of Turing systems have been found in many developmental processes, including the patterning signaling of digits, feathers, hairs, intestinal villus, rugae, turtle shells, and others (Sharpe, 2017; Raspopovic et al., 2014; Moustakas-Verho et al., 2014; Economou et al., 2012; Glover et al., 2017; Walton et al., 2015). In the case of planarian regeneration, a Turing system forming a graded anterior-posterior expression of head or tail morphogen signal can maintain and repattern itself after amputations (Meinhardt, 1982; Meinhardt, 2009). In addition, it has been suggested that the scale-free property of planarian worms where the head-tail gradient patterns are maintained at different worm lengths are due to an additional expander morphogen controlling the reaction-diffusion system (Werner et al., 2015), yet this system cannot explain the fission in planaria. Importantly, Turing systems can account for the dynamic insertion and spacing of the pattern peaks in growing domains (Crampin et al., 2002; Crampin et al., 2002; Crampin et al., 1999) as it has been shown in models of hydra budding, fish pigmentation, teeth primordia, and digit formation (Meinhardt, 1993; Kondo and Asai, 1995; Kulesa et al., 1996; Miura et al., 2006).

Molecular assays have shown several genes in planaria forming anterior-posterior expression gradients (Sureda-Gómez et al., 2016; Lander and Petersen, 2016), which can represent the molecular basis of the Turing system controlling the head and tail pattern. The Wnt/β-catenin signaling pathway form tail-to-head gradients while the ERK/FGFRL signaling pathway form head-to-tail gradients, both being essential for the correct patterning of the anterior-posterior axis in planaria (Lander and Petersen, 2016; Scimone et al., 2016; Umesono et al., 2013; Umesono, 2018). RNAi of β-catenin prevents the regeneration of tails and results in double-head worms (Gurley et al., 2008; Iglesias et al., 2008; Petersen and Reddien, 2008) whereas its inhibition with RNAi of APC prevents the regeneration of heads and results in double-tail worms (Gurley et al., 2010). Molecular evidence shows that the head-signaling or the tail-signaling gradients are maintained even in RNAi-treated double-head and double-tail worms, respectively, which suggests that these two gradients are auto-regulated independently and mutually inhibited (Stückemann et al., 2017). From a formalized dataset of planarian regenerative functional experiments (Lobo et al., 2013; Lobo et al., 2013), a dynamic spatial model comprising the regulation of 7 essential genes was reverse-engineered to be able to recapitulate the regeneration dynamics after amputations, genetic knock-downs, and pharmacological interventions (Lobo and Levin, 2015; Lobo and Levin, 2017) and predict novel signaling pathways in planarian regeneration (Lobo et al., 2016).

Here we propose that a Turing system can self-regulate the anterior-posterior opposite head and tail gradients in planaria for not only its maintenance and repatterning after amputations, but also for the signaling of fission. We show that a cross-inhibited Turing mechanism in a growing domain can self-regulate to insert new intercalated tail and head peaks, which signals when and where the worm fissions. Furthermore, a control signal produced anteriorly by the head morphogen can regulate the length scale of the Turing system, and explain the asymmetry of the resulting head and tail fragments, the induction of fission by anterior amputations in short worms, the multiple consecutive fissions during fragmentation, and the effects of environmental factors on fission. We mathematically analyze the proposed model and show with numerical simulations its predictive power for when and where planarian worms fission under different conditions.

2. A cross-inhibited Turing system explains the self-regulation of planarian fission

Introduced by Turing (1952), classical reaction-diffusion systems can form self-regulated patterns of graded and periodic high and low levels of expression. This mechanism can explain the planarian head and tail (Fig. 1A) self-regulated gradient signals with a peak in the anterior end, signaling the location of the head, and a peak in the posterior end, signaling the location of the tail, that can self-form, adjust to the length of the domain, and regenerate after perturbations such as amputations (Meinhardt, 1982; Schiffmann, 2011). In addition, the head and tail organizers must be independent in order to explain the double head and double tail phenotypes (Stückemann et al., 2017). Following the simplest version of the Gierer-Meinhardt kinetics in a one-dimensional domain with zero flux boundary conditions (Gierer and Meinhardt, 1972), such double Turing system (Fig. 1B) can take the form

$$\begin{aligned}
\partial_t a_H &= \frac{\mu_a\left(a_H^2+\rho\right)}{b_H} - \nu_a a_H + D_a\partial_x^2 a_H\\
\partial_t b_H &= \mu_b a_H^2 - \nu_b b_H + D_b\partial_x^2 b_H\\
\partial_t a_T &= \frac{\mu_a\left(a_T^2+\rho\right)}{b_T} - \nu_a a_T + D_a\partial_x^2 a_T\\
\partial_t b_T &= \mu_b a_T^2 - \nu_b b_T + D_b\partial_x^2 b_T,
\end{aligned} \tag{2.1}$$

where a_H and b_H are the activator and inhibitor of the head signaling, a_T and b_T are the activator and inhibitor of the tail signaling, respectively, μ_a and μ_b are the production rates, ν_a and ν_b are the decay rates, and D_a and D_b are the diffusion coefficients of the activators and inhibitors, respectively, and ρ is a basal production of the activators. This system forms a regular array of peaks and troughs in both the activators and inhibitor morphogens, forming periodic patterns with characteristic length scales for the activator and inhibitor depending on the diffusion and decay rates

$$\begin{aligned}
\lambda_a &= \sqrt{\frac{D_a}{\nu_a}},\\
\lambda_b &= \sqrt{\frac{D_b}{\nu_b}}.
\end{aligned} \tag{2.2}$$

This double Turing system can maintain a stable steady-state with non-overlapping head and tail peaks at each end of the domain, that correctly re-patterns after amputations forming new non-overlapping head and tail peaks at each end of the domain (Fig. 1B'). However, due to the constant length scale of the system, when the domain increases in size (as in a growing worm) the head and tail gradient patterns degenerate into patterns with overlapping peaks at both ends, and further growth forms overlapping peaks inserted in the middle of the domain (Fig. 1B").

As a solution for the loss of end peaks with growing domains in the classical Turing system, a self-scaling system have been pro-

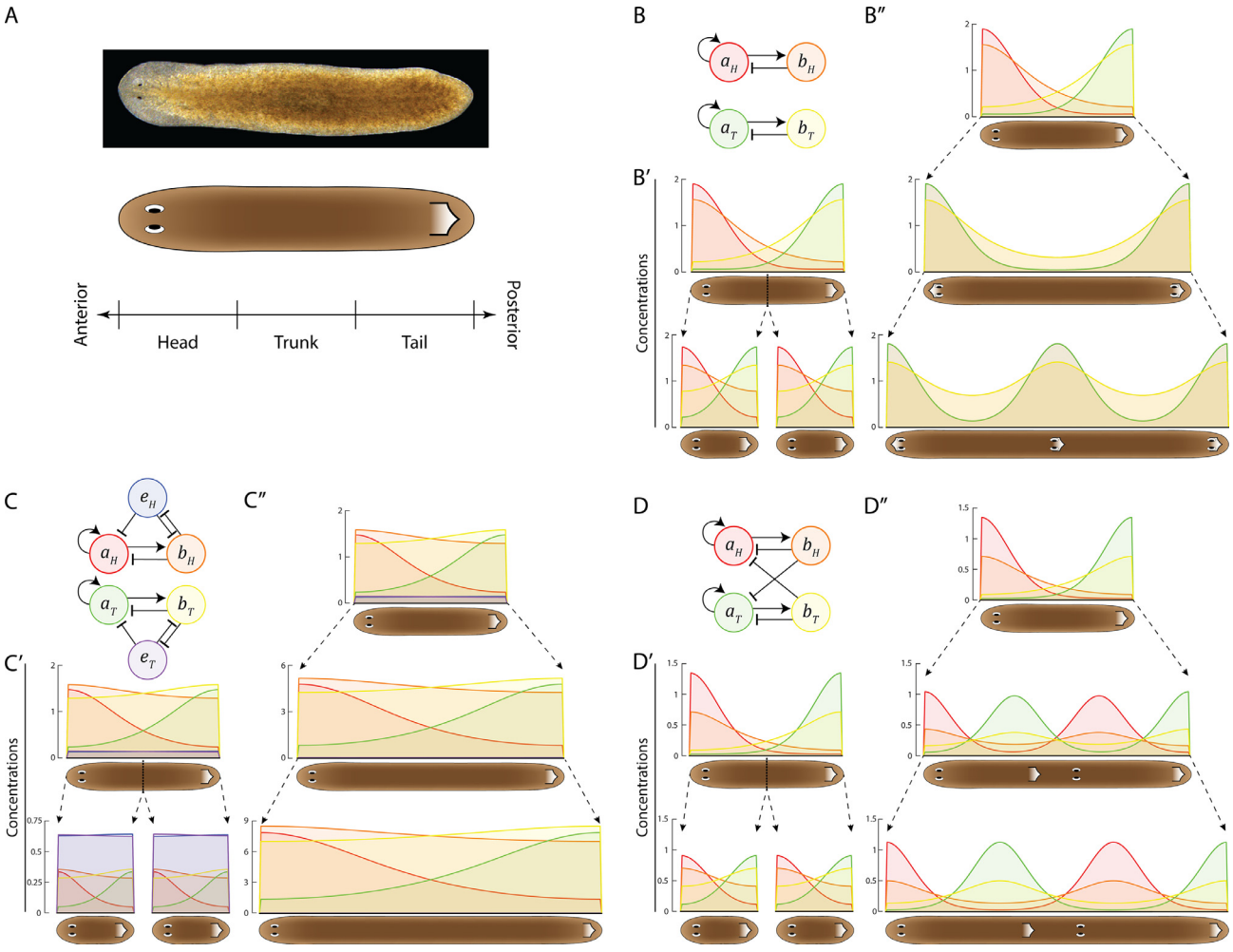

Fig. 1. Two independent Turing mechanisms can explain the planarian regeneration of opposite head (red) and tail (green) anterior-posterior morphogen gradients after an amputation, but a cross-inhibited Turing mechanism can additionally explain the fission signaling in a growing worm. (A) *Schmidtea mediterranea* planarian worm and its cartoon representation indicating body regions and anterior and posterior directions; cartoon eyes represent head and pointed shape represents tail. (B) A classic Turing system independently controlling opposite head and tail gradients can self-regenerate after a worm amputation (B'), but in a growing worm the two opposite gradients degenerate into an overlapping gradient with peaks at both the anterior and posterior ends (B''). (C) A Turing system with an expander scaling mechanism also regenerates the correct head and tail gradient patterns after an amputation (C'), but although it maintains the correct opposite head and tail gradient patterns in a growing worm, it cannot predict the signal for fission when the worm reaches a certain length (C''). (D) A cross-inhibited Turing system regenerates the correct pattern after an amputation (D') and correctly predicts the fission signaling in a growing worm by producing two new intercalated tail and head peaks when the worm reaches a certain length (D''). Morphogens: a_H head activator, b_H head inhibitor, a_T tail activator, b_T tail inhibitor. Parameters: (B) μ_a, $\nu_a = 0.1$, $\mu_b, \nu_b = 1$, $\rho = 0.01$, $D_a = 0.001, D_b = 0.1$; (C) as in (Werner et al., 2015); (D) $\sigma = 5$, all others as in (B). Units are arbitrary.(For interpretation of the references to colour in this figure legend, the reader is referred to the web version of this article.)

posed for planarian worms (Werner et al., 2015). The classical Turing system is extended with an expander morphogen inhibited by the inhibitor, and that inhibits both the activator and inhibitor. Following the original formulation based on Hill equations, this system can be implemented independently for both the head and tail gradients (Fig. 1C) with

$$\begin{aligned}
\partial_t a_H &= \frac{\mu_a a_H^h}{a_H^h + b_H^h} - \nu_a e_H a_H + D_a \partial_x^2 a_H \\
\partial_t b_H &= \frac{\mu_b a_H^h}{a_H^h + b_H^h} - \nu_b e_H b_H + D_b \partial_x^2 b_H \\
\partial_t e_H &= \mu_e - \nu_e b_H e_H + D_e \partial_x^2 e_H \\
\partial_t a_T &= \frac{\mu_a a_T^h}{a_T^h + b_T^h} - \nu_a e_T a_T + D_a \partial_x^2 a_T \\
\partial_t b_T &= \frac{\mu_b a_T^h}{a_T^h + b_T^h} - \nu_b e_T b_T + D_b \partial_x^2 b_T \\
\partial_t e_T &= \mu_e - \nu_e b_T e_T + D_e \partial_x^2 e_T,
\end{aligned} \tag{2.3}$$

where e_H and e_T are the expanders for the head and tail systems, respectively, μ_e, ν_e, and D_e are the production, decay, and diffusion rates for the expanders, respectively, and h is the Hill coefficient.

The self-scaling Turing system can maintain and regenerate the correct gradients after amputations as in the classical system (Fig. 1C'), but it prevents the merging of the head and tail peaks in a growing domain by proportionally scaling the head and tail gradients (Fig. 1C''). This scaling is due to the decrease of the expander concentration with domain length, which decreases the effective decay rates of the activators and inhibitors, resulting in a proportional increase in length scale (Eq. (2.2)). However, since the system scales over several orders of magnitude, it cannot produce new head and tail peaks when the domain reaches a certain length—the mechanism we suggest here as responsible for the planarian fission.

We propose a cross-inhibited Turing system for the signaling of planarian fission. The cross-inhibition can be formulated in the classical reaction-diffusion system by inhibiting the head activator with the tail inhibitor, and, conversely, inhibiting the tail activator

with the head inhibitor (Fig. 1D). Extending Eq. (2.1), this system takes the form

$$\begin{aligned}\partial_t a_H &= \frac{\mu_a\left(a_H^2+\rho\right)}{b_H(1+\sigma b_T)} - \nu_a a_H + D_a\partial_x^2 a_H\\ \partial_t b_H &= \mu_b a_H^2 - \nu_b b_H + D_b\partial_x^2 b_H\\ \partial_t a_T &= \frac{\mu_a\left(a_T^2+\rho\right)}{b_T(1+\sigma b_H)} - \nu_a a_T + D_a\partial_x^2 a_T\\ \partial_t b_T &= \mu_b a_T^2 - \nu_b b_T + D_b\partial_x^2 b_T,\end{aligned} \tag{2.4}$$

where σ modulates the strength of the cross-inhibition. The classic Turing system (2.1) is a special case of this generalized system when $\sigma = 0$.

Like the classic system, the cross-inhibited Turing system can maintain and regenerate the correct opposite head and tail gradients after amputations (Fig. 1D'). However, in a growing domain the patterns do not merge into overlapping peaks, but they are correctly maintained in the opposite ends of the anterior-posterior axis. Furthermore, when the growing domain reaches a critical length, a new pair of intercalated tail and head peaks form between the original head and tail peaks at opposite ends (Fig. 1D''). Here we propose that these new tail and head peaks forming two sequential head-tail gradient patterns are precisely the self-regulated signals that produce the fission in planaria. These new sequential tail and head signal peaks located midway along the anterior-posterior axis can represent the early signals for the development of tail and head morphological structures in the trunk region, which then trigger all the biomechanical mechanisms that execute the self-tearing during fission due to an ectopic tail signal anterior to a head signal and, vice versa, an ectopic head signal posterior to a tail signal. In this way, the cross-inhibited Turing system is the main regulator of when and where planaria fission.

3. Analysis of the cross-inhibited Turing system

A Turing system forms spatial patterns when it exhibits diffusion-driven instability, also called Turing instability. For this, the system without diffusion must be stable in the homogeneous steady state and the system with diffusion unstable to small spatial perturbations (Murray, 2003). To test these stability conditions, we use classic linear stability analysis of the system about the equilibrium state.

We generalize a Turing system in one spatial dimension, such as (2.4), with

$$\partial_t \mathbf{c} = \mathbf{f}(\mathbf{c}) + \mathbf{D}\partial_x^2\mathbf{c}, \tag{3.1}$$

where $\mathbf{c}$ is the morphogens vector, $\mathbf{f}$ is the production and decay rate equations, and $\mathbf{D}$ is the diagonal matrix of the diffusion rates for each morphogen. Let $\mathbf{c}_0$ be a homogeneous steady state of (3.1) such that $\mathbf{f}(\mathbf{c}_0) = 0$. Linearizing about the steady state $\mathbf{c}_0$, we set a perturbation $\mathbf{w} = \mathbf{c} - \mathbf{c}_0$ and, with $|\mathbf{w}|$ being small, (3.1) becomes

$$\partial_t \mathbf{w} = \mathbf{J}\mathbf{w} + \mathbf{D}\partial_x^2\mathbf{w}, \tag{3.2}$$

where $\mathbf{J}$ is the Jacobian matrix of $\mathbf{f}$ with respect $\mathbf{c}$ evaluated at the steady state $\mathbf{c} = \mathbf{c}_0$.

Analyzing the long term behavior of the perturbation, we can determine the stability of the system in the absence and presence of diffusion (Baker et al., 2008; Smith and Dalchau, 2018). On a domain $x \in [0, L]$ with zero-flux boundary conditions, the solutions of (3.2) take the form

$$\mathbf{w} = \mathbf{w}_0 e^{\lambda t}\cos kx,\ k = 0, \frac{\pi}{L}, \frac{2\pi}{L}, \frac{3\pi}{L}, \ldots \tag{3.3}$$

where λ are the eigenvalues of $\mathbf{J}$ and k are the wavenumbers of the eigenmode. Substituting Eq. (3.3) into (3.2) and cancelling $e^{\lambda t}\cos kx$ results in

$$\lambda\mathbf{w}_0 = \mathbf{J}\mathbf{w}_0 - k^2\mathbf{D}\mathbf{w}_0, \tag{3.4}$$

which simplifies into

$$\left(\lambda\mathbf{I} - \mathbf{J} + k^2\mathbf{D}\right)\mathbf{w}_0 = 0. \tag{3.5}$$

The nontrivial solutions for the eigenvalues λ can be determined with the characteristic polynomial

$$\left|\lambda\mathbf{I} - \left(\mathbf{J} - k^2\mathbf{D}\right)\right| = 0, \tag{3.6}$$

which roots are the eigenvalues of $\mathbf{J} - k^2\mathbf{D}$. We then can use the dispersion relation to find the eigenfunctions that are linearly unstable. Denoting by $\sigma_{\mathbf{J}-k^2\mathbf{D}}$ the spectrum of eigenvalues of $\mathbf{J} - k^2\mathbf{D}$, the dispersion relation becomes

$$h\left(k^2\right) := \max\left\{\Re\left(\sigma_{\mathbf{J}-k^2\mathbf{D}}\right)\right\}. \tag{3.7}$$

The two conditions for the system to exhibit diffusion-driven instability and hence form Turing patterns are $h(0) < 0$, that is that the real part of the eigenvalues at $k = 0$ are all negative, for the system without diffusion to be stable in the homogeneous steady state, and $\exists k^* \neq 0 | h(k^*) > 0$, that is the existence of at least one wavenumber $k^* \neq 0$ with a corresponding eigenvalue λ^* with a positive real part, for the system with diffusion to be unstable.

We apply this stability analysis to the cross-inhibited Turing system (2.4). Fig. 2A shows the bifurcation diagrams of the system with different values of cross-inhibition strength σ when varying the inhibitors diffusion constant, D_b, and decay constant, ν_b, over large ranges. The light blue regions correspond to systems that fulfill the first condition for Turing instability ($h(0) < 0$) but not the second ($\exists k^* \neq 0 | h(k^*) > 0$), while the dark blue regions correspond to systems that fulfill both conditions and hence form Turing patterns. Notice that when the cross-inhibition strength $\sigma = 0$, the cross-inhibited Turing system degenerates into the classical Turing system (2.1). The results show that adding the cross-inhibition to the classical Turing system alters the boundary of the parameter space that leads to patterns, yet many parameters form patterns in both systems.

We next numerically analyze the basins of attractions of the cross-inhibited Turing system in a growing domain. Starting with a stable and opposite head and tail gradients, we simulate the worm growth by increasing the domain length at a constant speed, slow enough to reach the basin of attraction at each length. Fig. 2B shows the patterns formed by the system in the growing domain varying the cross-inhibition strength σ and a length scale factor γ. With cross-inhibition strength $\sigma = 0$, the system degenerates to the classical Turing system (2.1), and the opposite head and tail gradients develop into overlapping gradients, as shown in Fig. 1B''. The same behavior occurs with weak cross-inhibition strengths, and the patterns become more transient at longer domains. At cross-inhibition strengths of 1 and above, the system follows the same transition from an opposite head and tail gradients pattern to the intercalated head-tail, head-tail gradients pattern at a specific domain length. Varying the length scale of the system by a factor γ, equally dividing both inhibitor parameters ($\nu_a^* = \frac{\nu_a}{\gamma}$, $\nu_b^* = \frac{\nu_b}{\gamma}$), results in the basins of attraction being displaced and the formation of the new intercalated head and tail peaks being moved towards longer domains.

4. Fission induced by intercalation of new tail and head gradient peaks

We demonstrate how the sequential tail and head gradient peaks inserted in the middle area of the anterior-posterior axis by the cross-inhibited Turing system can signal planarian fission. For this, the simulation now includes an automatic domain fission at

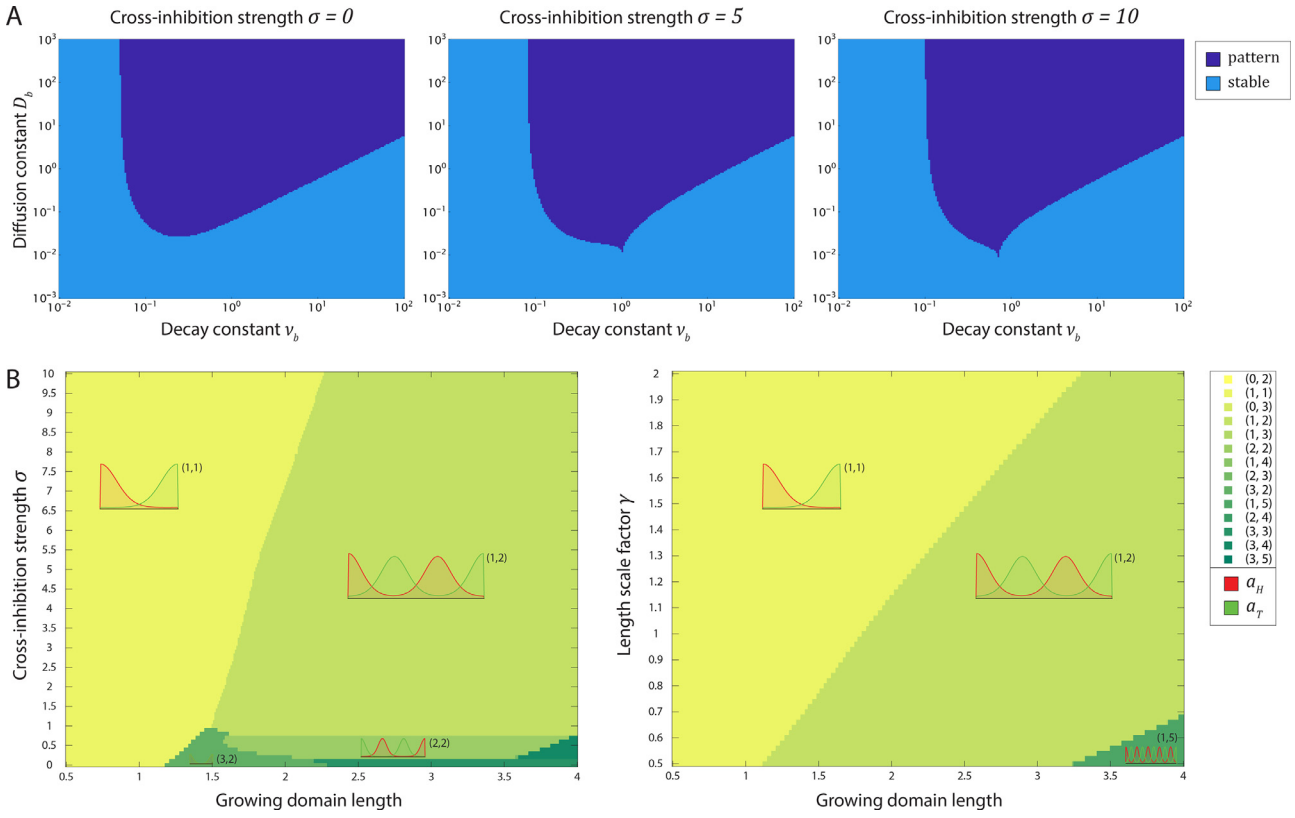

Fig. 2. Analysis of the cross-inhibited Turing system. (A) Bifurcation diagrams for different cross-inhibition strength σ. The light blue region indicates parameter values for which the homogeneous equilibrium is stable; the dark blue region indicates parameter values forming a diffusion-driven instability and hence forming a Turing pattern. (B) Basins of attraction in a growing domain from 0.5 to 4 units of length and starting with opposite head-tail gradients in steady state, with respect cross-inhibition strength σ and length scale factor γ. Pattern numbers (m,n) indicate whether the head morphogen has a peak touching both ($m = 3$), only the posterior ($m = 2$), only the anterior ($m = 1$), or none ($m = 0$) of the boundaries, and the total number of head peaks in the pattern (n). Unless otherwise noticed, parameters values as in Fig. 1D.(For interpretation of the references to colour in this figure legend, the reader is referred to the web version of this article.)

the middle point between any sequential anterior-to-posterior tail-head gradient peaks self-formed by the model (a peak is considered formed when it reaches at least 75% of the morphogen range). Fig. 3A shows such a simulation in a growing domain. New tail and head peaks form in the center area when the worm reaches a certain length, which automatically triggers the fission of the domain at the midpoint between the new tail and head peaks. Following fission, the correct opposite head and tail gradients are self-regenerated in the resulting new two worms.

In a growing domain, the process of fission is triggered recurrently, as shown in Fig. 3B with a continuous plot of the head and tail activator levels along a growing domain over one order of magnitude. New tail and head peaks are formed around the center of the domain, which then triggers the fission of the domain whenever the domain reaches a certain length (about 1.5 units of length with these parameters—arbitrary units). After each fission, the two new head and tail gradients self-adapt to the new domain lengths, and their peaks shift to the opposite ends of the domain. Three rounds of fission are shown. Fig. 3C shows cartoon diagrams of the planarian worm morphology corresponding to the expression patterns and fissions in Fig. 3B. In this simulation, only the most anterior and posterior domains grow, and hence only the worms representing those domains fission.

5. A delayed control mechanism for the cross-inhibited Turing system explains the induction of fission after anterior amputations and asymmetrical fission in posterior locations

Anterior amputations in planaria, but not posterior, induce fission even in worms of short length, a behavior that can be recapitulated by the cross-inhibited Turing system by introducing a delayed control mechanism. A morphogen being produced in the anterior region—possibly by the head activator—can control the length scale of the system by inhibiting the degradation of both the activator and inhibitor morphogens (an alternative mechanism could be to enhance the diffusion constants). In this way, an anterior amputation removes the anterior region, which produces the control morphogen, and hence results in the decrease of the expression levels of the control morphogen. The lower level of this signal reduces the length scale of the system, which induces the formation of new tail and head peaks, since the number of peaks is proportional to the length scale of the system. These new peaks trigger the fission of the worm, even when its length is short. It is important that the control morphogen is restored slower than the anterior head signals that produce it, so there is enough time for the system to maintain the shorter length scale and produce the new tail and head peaks that result in fission.

The cross-inhibited Turing system in (2.4) can be extended with this delayed control mechanism by adding a control morphogen c being produced by the head activator a_H through a signaling component d that does not diffuse and act as a delay (other delay mechanisms not needing an additional component are also possible). The control morphogen c inhibits the decay of the activator and inhibitor morphogens, effectively modulating the length scale of the Turing system. Fig. 4A shows a diagram of the mechanism. Extending the system in (2.4), the equations for the controlled cross-inhibited Turing system become

$$\partial_t a_H = \frac{\mu_a\left(a_H^2+\rho\right)}{b_H(1+\sigma b_T)} - \frac{\nu_a a_H}{1+\tau c} + D_a\partial_x^2 a_H$$

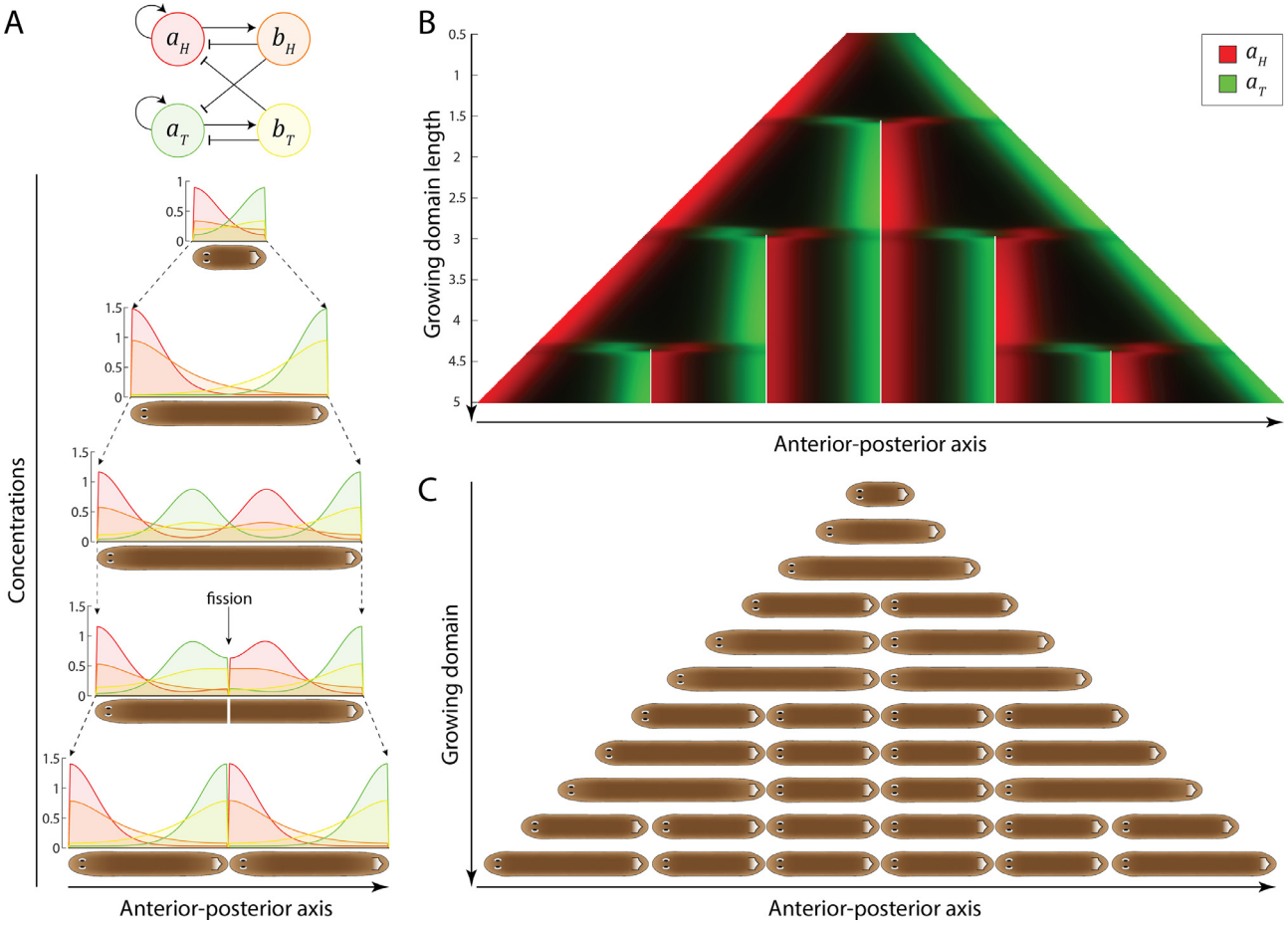

Fig. 3. The self-regulatory dynamics of a cross-inhibited Turing system controls when and where the fission occurs. (A) The cross-inhibited Turing system forms itself new tail (green) and head (red) activator peaks between the end peaks when a growing worm reaches a certain length, which automatically signals the fission of the worm. The interface between the new tail and head peaks signals the time and location of the fission plane, which divides the growing domain into two. After fission, the head and tail gradient patterns self-adapt to their correct shapes due to the new lengths of the two newly formed domains. (B) Head and tail activator levels in a growing domain from 0.5 to 5 units of length signal multiple rounds of fission. New tail and head peaks form and automatically signal the fission of the worm when the domain reaches a length of 1.5 units. (C) Diagram showing the worm morphology corresponding to the head and tail activator levels in the growing domain depicted in panel (B). Parameters values as in Fig. 1D.(For interpretation of the references to colour in this figure legend, the reader is referred to the web version of this article.)

$$
\begin{aligned}
\partial_t b_H &= \mu_b a_H^2 - \frac{\nu_b b_H}{1+\tau c} + D_b \partial_x^2 b_H \\
\partial_t a_T &= \frac{\mu_a\left(a_T^2+\rho\right)}{b_T(1+\sigma b_H)} - \frac{\nu_a a_T}{1+\tau c} + D_a \partial_x^2 a_T \\
\partial_t b_T &= \mu_b a_T^2 - \frac{\nu_b b_T}{1+\tau c} + D_b \partial_x^2 b_T \\
\partial_t c &= \mu_c d^2 - \nu_c \mathrm{c} + D_c \partial_x^2 \mathrm{c} \\
\partial_t d &= \mu_d a_H^2 - \nu_d \mathrm{d},
\end{aligned}
\tag{5.1}
$$

where μ_c and μ_d are the production rates and ν_c and ν_d are the decay rates of the control morphogen and delay component, respectively, D_c is the diffusion coefficient of the control morphogen, and τ is the strength of the control signal. The system (2.4) is a particular case of the system (5.1) when $\tau = 0$.

The controlled cross-inhibited Turing system behaves similarly to the simple cross-inhibited Turing system in a growing domain but induces fission after an anterior amputation. Fig. 4B shows how the system inserts new intercalated tail and head peaks that signal fission when the domain reaches a certain length (about 2 units of length with these parameters). However, an anterior amputation induces the formation of new intercalated tail and head peaks that signal fission, as shown in Fig. 4C. After the amputation, the worm is about 1 unit of length, yet new tail and head peaks form at this length, which is half the length of fission of an intact worm. This is due to the decay of the controller morphogen, since the head activator peak—its indirect regulatory enhancer through the delay component—was removed with the amputation. A lower concentration level of the controller morphogen decreases the length scale of the Turing system, which induces the formation of new intercalated tail and head peaks, signaling fission even in a short worm.

Planarians can fission asymmetrically, resulting in a longer anterior fragment and a shorter posterior fragment. The controlled cross-inhibited Turing system can recapitulate this behavior when the length scales of the head and tail Turing systems are different. Since the controller morphogen c modulates the length scales of both Turing systems, model parameters resulting in a concentration gradient of c can produce asymmetric fissions. Fig. 5 shows how the controller c forming a concentration gradient due to a slower diffusion parameter D_c can induce fission with a posterior fragment length 40%, 30%, or 20% of the total worm length depending on the control strength τ (due to the asymmetrical expression levels, here a peak is considered formed when it reaches at least 40% of the morphogen range). This posterior fission is due to the asymmetry of the length scale of the Turing system, which is higher anteriorly due to the higher levels of the controller morphogen and lower posteriorly due to the lower levels of the controller morphogen.

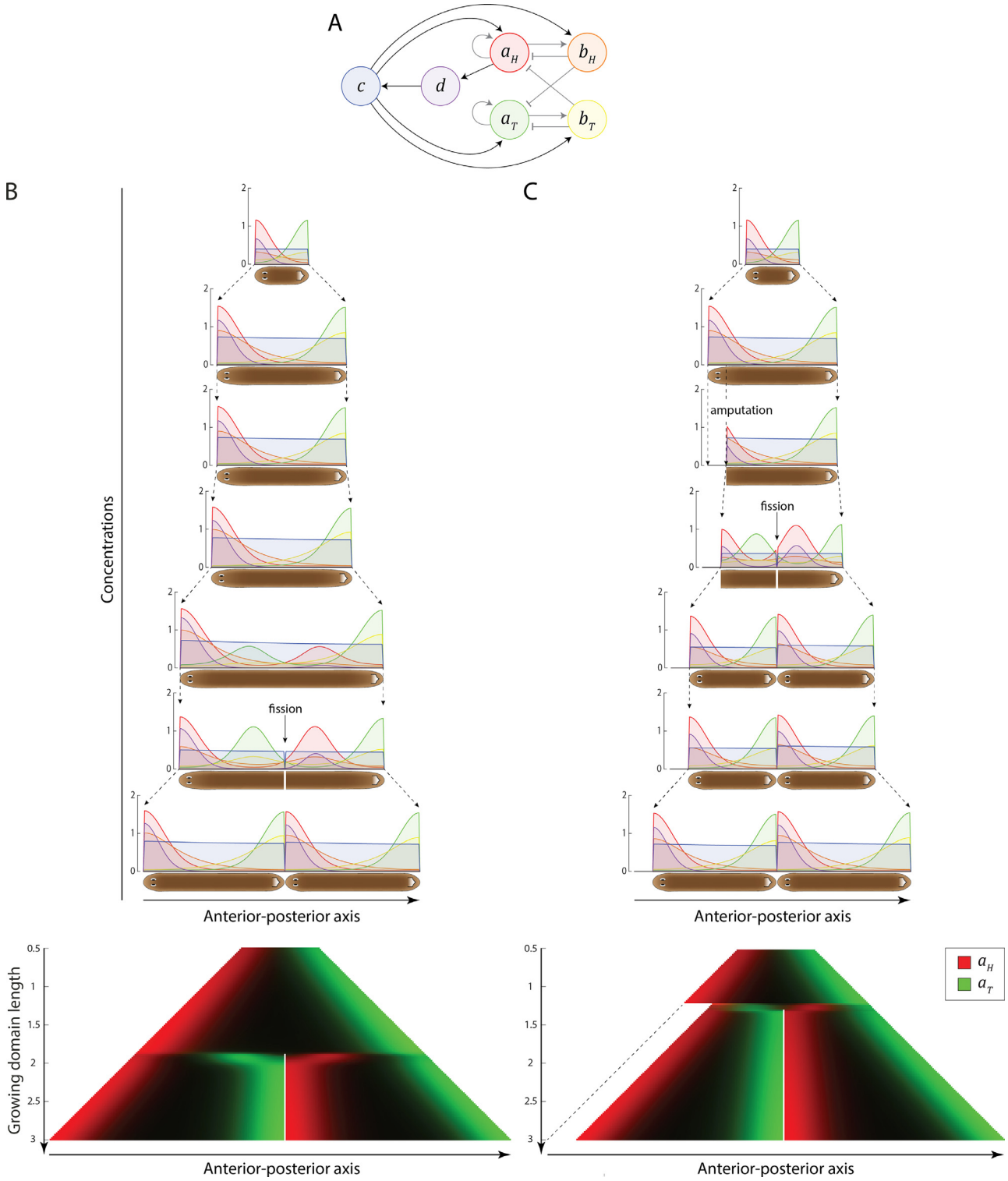

Fig. 4. A delayed mechanism controlling the cross-inhibited Turing system regulates the length scale of the system and explains the induction of fission with anterior amputations. (A) A fast-diffusible morphogen c enhances the production of all the morphogens in the head and tail Turing systems and is produced by the head activator a_H through a slowly expressed non-diffusible species d, representing a different component in the signaling pathway or the delay in the transcription and translation of the controller c. (B) Similar to the cross-inhibited Turing system, in an intact growing worm new head and tail peaks are formed, and hence fission is signaled when the worm reaches about 2 units of length. (C) However, an anterior amputation induces the formation of new head and tail peaks and hence fission, even in shorter worms of 1.25 units of length. This early induction is due to the decay of the controller morphogen c after the anterior amputation removes the anterior peak of the head morphogen a_H, which results in the Turing system length scale being decreased and hence the formation of new tail and head peaks in a shorter worm. Parameters values as in Fig. 1D, except: $\nu_a = 0.5$, $\nu_b = 5$, $\mu_c = 5$, $\nu_c = 1$, $\mu_d = 0.05$, $\nu_d = 0.1$, $\tau = 5$, $D_c = 10$.

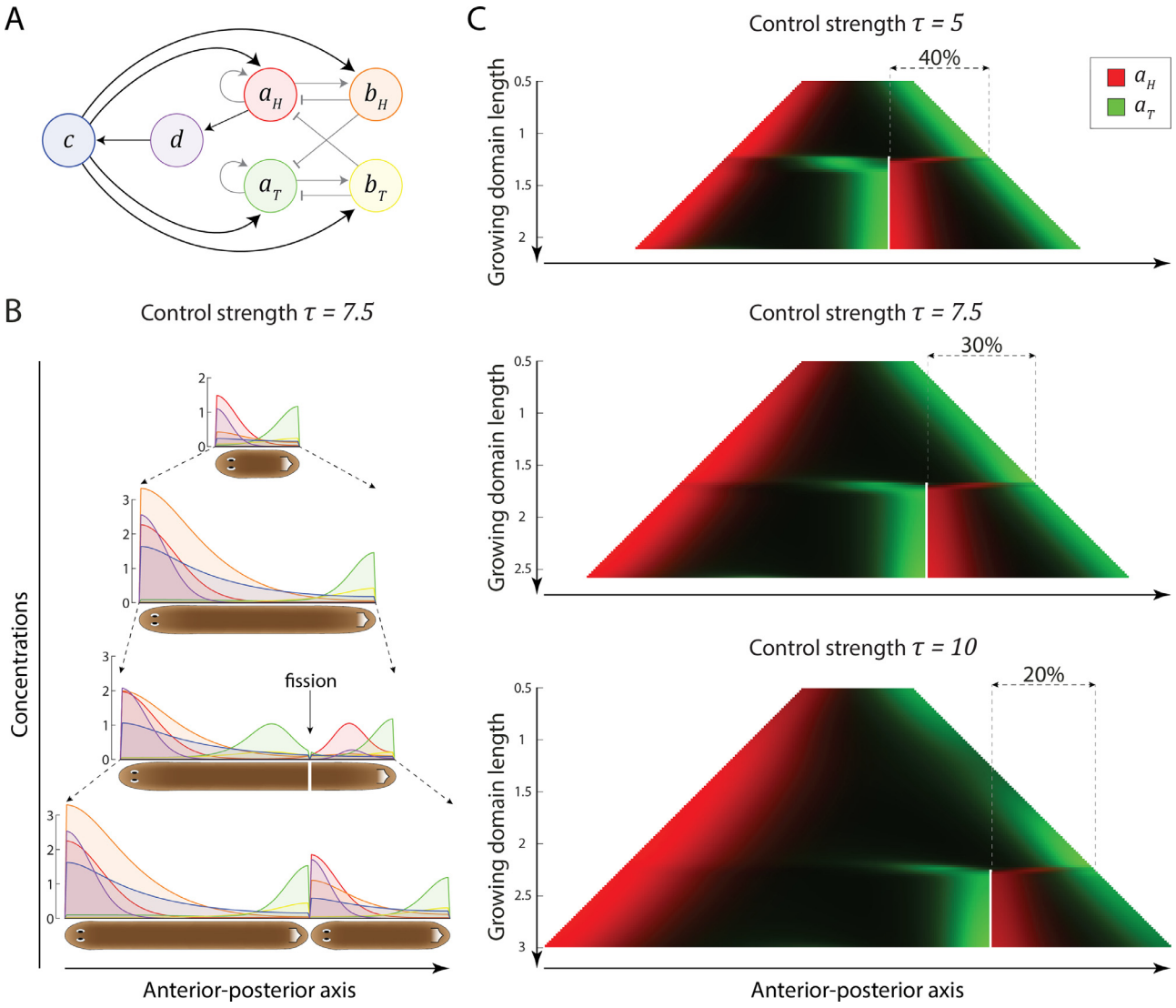

Fig. 5. Fission is induced in a more posterior location when the controller morphogen c forms a concentration gradient. (A) A lower-expressed and slower-diffusible controller morphogen c results in a concentration gradient with an anterior peak. (B) The concentration gradient of c results in the formation of new tail and head peaks in a more posterior location, and hence the fission of asymmetrical fragments due to the Turing system length scale being higher anteriorly and lower posteriorly. (C) A higher control strength τ produces fission in a more posterior location. Parameters values as in Fig. 4, except: $\mu_c = 1$, $D_c = 0.2$, and τ as noticed.

6. Analysis of the controlled cross-inhibited Turing system

We apply the stability analysis to the controlled cross-inhibited Turing system (5.1). Fig. 6A shows the bifurcation diagrams of the system with different values of cross-inhibition strength σ when varying the inhibitors diffusion constant D_b and decay constant ν_b over large ranges. Like in the cross-inhibited Turing system, the addition of the controller pathway alters the boundary of the parameter space that leads to patterns, yet many parameters form patterns in both systems.

We next analyzed the basins of attraction in a growing domain starting with stable and opposite head and tail gradients. Increasing the control strength τ results in longer domains at which the worm forms the new intercalated tail and head peaks, and hence the length at which the worm fissions. This is due to the increasing of the system length scale when the control strength τ increases, since it is reducing the effective decay parameters in the head and tail activators and inhibitors. Varying the control morphogen production μ_c also changes with a positive correlation the length at which the worm forms the new intercalated tail and head peaks, and hence the length at which the worm fissions. This is because the direct effect of the morphogen production μ_c in the level of expression of the controller morphogen c, and hence a direct effect in the length scale of the Turing system.

7. Fragmentation due to a slower control mechanism

Planarian worms can also exhibit multiple fissions in a short time span, a behavior called fragmentation. The controlled cross-inhibited Turing system can recapitulate this behavior when the morphogens in the controller pathway are expressed at a lower rate, as shown in Fig. 7A. The original parameters produce a single fission in a growing domain from 0.5 to 3 units of length (Fig. 4B). However, Fig. 7B shows how parameters that slow down the control mechanism by reducing the production and decay rates of the controller morphogen and delay component result in two consecutive fissions, at total domain lengths of about 1.5 and 1.75 units of length. The slowing down of the controller mechanism reduces the length scale of the system, and hence multiple fissions occur sequentially—a fragmentation.

Further slowing down of the controller pathway with lower rates in the controller and decay morphogens increases the num-

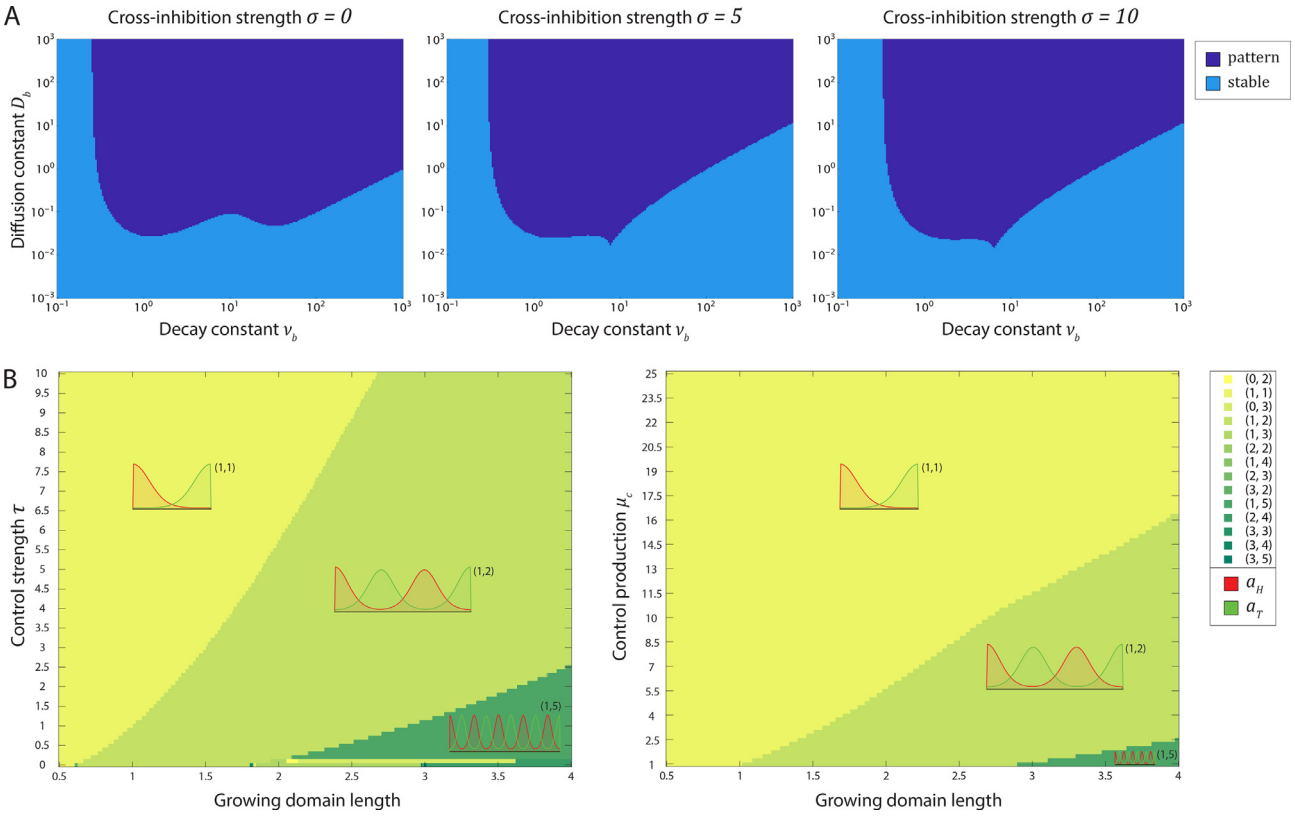

Fig. 6. Analysis of the controlled cross-inhibited Turing system. (A) Bifurcation diagrams for different cross-inhibition strength σ, showing the parameter ranges forming Turing patterns (dark blue), or just being homogenously stable (light blue). (B) Basins of attraction in a growing domain from 0.5 to 4 units of length and starting with opposite head-tail gradients in steady state, with respect control strength τ of the interaction between c and the cross-inhibited Turing system, and control production μ_c. Unless otherwise noticed, parameters as in Fig. 4.(For interpretation of the references to colour in this figure legend, the reader is referred to the web version of this article.)

ber of pieces during fragmentation. Fig. 7C shows the behavior of the system with such further slowdown, which results in three fissions in the same growth span of 0.5 to 3 units of length. In summary, the number of pieces obtained in a fragmentation depends on the levels of expression of the controller pathway, since it regulates directly the length scale of the Turing system.

8. Environmental factors affect fission through the controlled cross-inhibited Turing system

Several environmental factors can affect the fission behavior in planarian worms: high population density, high light intensity, or lower temperatures inhibits fission. These effects on fission by environmental factors can be explained through the control pathway in the cross-inhibited Turing system. By modulating the control production μ_c, through signals from the brain or physical alterations in molecular signals, the environmental factors can control the length at which the worm fissions or even prevent it altogether over a large range of worm lengths.

Fig. 8 shows the fission behavior of the controlled cross-inhibited Turing system with different levels of control production μ_c, simulating its regulation by environmental factors. When the population density or light intensity is low, or the temperature is high, the control production μ_c is expressed at a lower level (simulated with $\mu_c = 1$), which decreases the length scale of the system and hence increases the frequency of fission. Conversely, when the population density or light intensity is high, or the temperature is low, the control production increases its expression levels ($\mu_c = 5$) which lengthen the length scale of the system and hence lowers the frequency of fission. Higher expression levels due to the increase in control production ($\mu_c = 50$) can completely inhibit the fission of the worm over domain lengths of one order of magnitude.

9. Discussion

We proposed and analyzed here a mathematical model for the signaling of asexual reproduction by fission in planaria. A cross-inhibited Turing system can maintain opposite head and tail gradients, and then restore them in the correct locations after an amputation. This self-regulated system hence can account for the homeostasis and regeneration signaling of the head and tail morphological structures in planaria. Furthermore, in a growing domain this same mechanism produces at a specific length new intercalated tail and head peaks, which, similarly than after an amputation, induce the early signals for the development of tail and head morphological structures, but in the trunk region. We suggest that these new intercalated tail and head early signals and developmental structures trigger the biomechanical mechanisms that rip the worm into two pieces. Indeed, it has been long observed in planaria how “the new system gradually emerges from a part of the old” (Child, 1911), and how the anterior and posterior regions act independently before fission (Vandel, 1922). Moreover, an increase in neoblast proliferation similar than after an amputation has been observed in the fission area *before* the fission event (Bueno et al., 2002; Hori and Kishida, 1998) and inducing higher mitotic activity in neoblasts with RNAi of *DjP2X-A* results in a higher fission frequency (Sakurai et al., 2012). After fission, the same Turing mechanism repatterns the two independent pieces, shifting the newly-formed and opposite head and tail peak gradients towards the ends of the anterior and posterior regions, respectively. In this way,

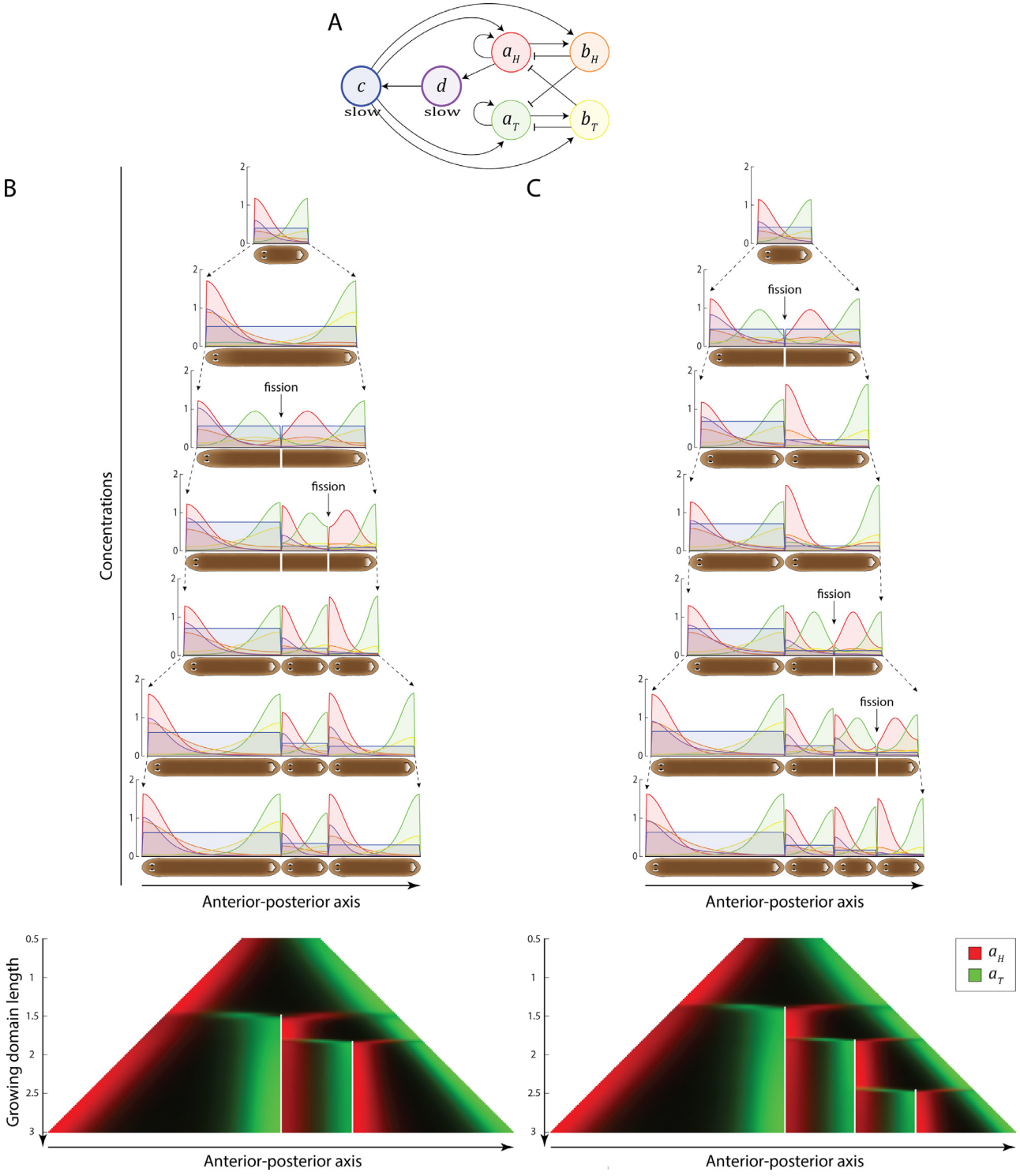

Fig. 7. A slower mechanism controlling the cross-inhibited Turing system produces worm fragmentations by further reducing the Turing system length scale, resulting in multiple sequential fissions. (A) Decreasing the production and decay constants in the control morphogens c and d slows the control mechanism of the cross-inhibited Turing system, which results in shorter length scales in the Turing system. (B) A slower control mechanism produces a fragmentation into three pieces in a growing domain from 0.5 to 3 units of length. Each of the resulting pieces regenerate the correct head (red) and tail (green) gradient patterns. (C) A further slower control mechanism produces a fragmentation into four pieces in the same growing domain, each of them regenerating the correct head-tail worm patterning. Parameters as in Fig. 4, except: $\mu_c = \frac{5}{50}$, $\nu_c = \frac{1}{50}$, $\mu_d = \frac{0.05}{25}$, $\nu_d = \frac{0.1}{25}$ in (B) and $\mu_c = \frac{5}{100}$, $\nu_c = \frac{1}{100}$, $\mu_d = \frac{0.05}{50}$, $\nu_d = \frac{0.1}{50}$ in (C).(For interpretation of the references to colour in this figure legend, the reader is referred to the web version of this article.)

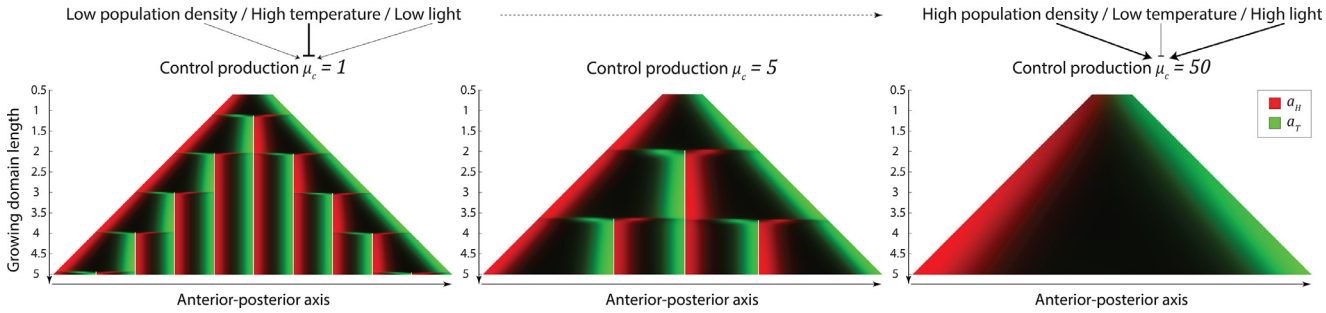

Fig. 8. Environmental factors can regulate the length at which the worm fissions by affecting the control production μ_c and hence the levels of expression of morphogen c, regulating the Turing length scale of the system. Population density and light intensity enhances the production of the control morphogen, whereas temperature inhibits it. A low population density, high temperature, and low light intensity environment lowers the production of the control morphogen, resulting in fission at about 1 unit of length. An environment with moderate levels results in fission at about 2 units of length. A high population density, low temperature, and high light intensity enhances the production of the control morphogen, resulting in no fission in worms below 5 units of length. Unless otherwise noticed, parameters as in Fig. 4.

the cross-inhibited Turing system specifies when and where planaria fission.

We demonstrated how a signal produced anteriorly controlling the length scale of the Turing system can explain the induction of fission with an anterior amputation even in short worms. As shown by the model, when the head activator is lost due to an anterior amputation, the control signal expression level decreases, resulting in a shortening of the length scale. If this signal is expressed with a delay with respect the head activator, the system forms new tail and head peaks in the trunk area, which results in the fission of the worm. This mechanism can also recapitulate the fragmentation in planaria when the control signal is expressed at slower rates. In this case, the length scale of the Turing system is not increased fast enough in the fissioned piece, resulting in two or more consecutive fissions. This mechanism may be responsible for the asexual reproduction by fragmentation observed in other organisms such as annelids, which can divide into 2 to 13 fragments (Myohara et al., 1999; Bely and Wray, 2001).

Different planarian species differ on their specific fission dynamics, such as length at fission, location of the fission plane, and number of consecutive fissions during fragmentation. We showed how the different parameters of the model can account for this variability by altering the effective regulation of the length scale of the Turing system. Depending on the gradient of the control morphogen, the model can account for both fission at the center or posteriorly towards the tail, which results in an asymmetric fission as observed in several species. An alternative model using different parameters for the head and tail Turing systems could also result in different length scales for each Turing system, and hence produce asymmetric fissions in a similar way. In addition, the internal organs in planaria, specially the intestines and pharynx in the trunk region, may alter the patterns of expression and diffusion dynamics of these signals, which may explain why planaria fission pre- or post- pharyngeal, but not through the pharynx.

Environmental factors affecting the planarian fission can be explained by a regulation of the control signal. In an environment with a low-density population, low light intensity, or high temperature the control signal may be expressed at lower levels, which shorten the length scale of the Turing system and hence increases the frequency of fissions. Conversely, an environment with high-density population, high light intensity, or low temperature may increase the expression levels of the control signal, which increases the length scale of the system and hence decreases the frequency of fissions, or even inhibits them altogether for a large range of lengths.

The interplay between the control mechanism and the cross-inhibited Turing system can explain the generational memory effect observed in anterior or posterior pieces during their next fission or fragmentation (Yang et al., 2017; Thomas et al., 2012; Quinodoz et al., 2011). Since the control morphogen is expressed anteriorly, a fissioned anterior piece may remain with a higher expression level of the control signal, resulting in a larger system length scale and hence an inhibition of fission. Conversely, a fissioned posterior piece contains lower expression levels of the control morphogen, and hence a shorter system length scale, which produces a second fission. Indeed, worms regenerated from posterior pieces fission again at shorter lengths than those regenerated from anterior pieces (Yang et al., 2017; Thomas et al., 2012; Quinodoz et al., 2011). However, the presented model is deterministic and hence cannot recapitulate the stochasticity found in planarian fission. Towards this goal, future work will extend the presented model with stochastic Turing systems on growing domains (Woolley et al., 2011).

The morphogens of the presented Turing system have several molecular candidates, since many gene expression patterns are known to form independent but antagonistic gradients with peaks in the head or the tail (Stückemann et al., 2017) as predicted by the proposed model. The activator in the head Turing system (a_H) can be a member of the ERK/FGFRL signaling pathway, such as an FGF-like ligand of receptor *ndk, ndl-1, ndl-4*, or *ndl-5*, all forming anterior expression peaks (Lander and Petersen, 2016; Umesono et al., 2013). The inhibitor in the head Turing system (b_H) can be members of the Wnt/β-catenin signaling pathway inhibiting other members of the Wnt pathway to form the cross-inhibitory link, such as *notum, sFRP-1*, or *foxD*, all forming anterior expression peaks (Scimone et al., 2016). The activator (a_T) and inhibitor (b_T) in the tail Turing system can be secreted proteins of the Wnt/β-catenin signaling pathway, such as *wnt1, wnt11-1*, and *wnt11-2*, all forming posterior expression peaks and having positive and negative interactions between them (Reddien, 2018). Importantly, members of both FGFRL and Wnt signaling pathways have been found to form developmental Turing systems in other organisms (Marcon and Sharpe, 2012). The proposed delayed control mechanism can be implemented with members of the ERK/FGFRL signaling pathway, where the fast-diffusible controller c can be a FGF-like ligand and the non-diffusible delay component d a FGF-like receptor such as *ndk*, both forming anterior peaks (Cebrià et al., 2002).

In addition to molecular mechanisms, periodic patterns similar to reaction-diffusion Turing systems can be realized with cellular or mechanical mechanisms including non-linear local activation and long-range inhibition to produce a periodic pattern and control its length scale (Brinkmann et al., 2018). Hence, the components of the proposed cross-inhibition Turing system could be at least partially based on cellular properties such as differential cell movements as in zebrafish pigment cells (Nakamasu et al.,

Table 1
Proposed validation experiments to test the cross-inhibited Turing system model and elucidate its possible physical implementation.

Hypothesis	Experiment	Predicted outcome
Molecular components	*In situ* hybridization of ERK/FGFRL and Wnt pathways components (Stückemann et al., 2017)	Pre-fission intercalated high-low-high-low expression pattern for head genes and vice versa for tail genes
	RNAi of ERK/FGFRL pathway components (Lander and Petersen, 2016; Umesono et al., 2013)	Increase/decrease in fission frequency
	RNAi of Wnt pathway components (Scimone et al., 2016)	Increase/decrease in fission frequency (validated in (Arnold et al., 2019))
	RNAi of FGF-like ligands or *ndk* (controller/delay) (Cebrià et al., 2002)	Increase in fission frequency
Cellular components	Reduction of cell motilities (Endo et al., 2005) or lifetime (Pellettieri et al., 2010)	Decrease in fission frequency
	Reduction on length of cellular protrusions (Zeng et al., 2018)	Decrease in fission frequency
Mechanical components	RNAi of cellular collagen and glycoproteins (Cote et al., 2019)	Decrease in fission frequency
Bioelectrical components	Membrane voltage reporter assay (Beane et al., 2011; Beane et al., 2013)	Pre-fission intercalated de-hyper-de-hyper-polarized voltage pattern
	Ion transport inhibitors (Beane et al., 2011) or gap junction blockers (Emmons-Bell et al., 2015)	Increase/decrease in fission frequency
Fission induction signals	Neural markers (Ross et al., 2017) or tracer injections (Lerner et al., 2016)	Pre-fission early cephalic ganglia formation posterior to the fission plane
	Grafting of trunk and head pieces into the trunk region (Kobayashi et al., 1999)	Induction of fission

2009) or cell contacts through filopodia as in *Drosophila* bristles (Cohen et al., 2010), or mechanical tissue properties such as rigidity or elasticity (Mercker et al., 2013) as in hydra body axis regeneration (Livshits et al., 2017; Mercker et al., 2015). Bioelectrical mechanisms can also produce and perturb anterior-posterior patterns and participate in the control of planarian regeneration (Durant et al., 2016; Lobo et al., 2014), which suggests the presence of a bioelectricity-integrated gene and reaction controlling network (Pietak and Levin, 2017).

Elucidating the molecular, cellular, or mechanical physical realization of the proposed cross-inhibited Turing system could be accomplished with targeted perturbations for each type of physical mechanism to alter the length scale λ_a and λ_b of the system (Eq. (2.2)) (Hiscock and Megason, 2015) and observing the predicted change on the minimal worm length that fissions, as shown in Fig. 2. Table 1 summarizes a set of possible experiments to test the proposed model and its physical realization. Before fission occurs, the model predicts the presence of intercalated tail and head signal peaks around the plane of fission. A molecular mechanism could be tested using *in situ* hybridization to obtain the gene expression patterns of the ERK/FGFRL signaling pathway and the Wnt/β-catenin signaling pathway before and during the fission of planaria and observe whether the components with anterior peaks form them anew posterior to the fission plane and those with posterior peaks form them anew anterior to the fission plane. Knock downs of ERK/FGFRL and Wnt pathway components forming the proposed cross-inhibited Turing system are predicted to alter the fission frequency of the worm, depending on the positive or negative influence on the length scale (Eq. (2.2)). Indeed, it has been shown recently that knock-downs of activators in the Wnt pathway (*wnt11-6, dsh-B, β-catenin*, or *tsh* RNAi) reduces the frequency of fission, while knock-down of an inhibitor in the Wnt pathway (*apc* RNAi) increases the frequency of fission (Arnold et al., 2019). In addition, knock-downs of FGF-like ligands or *ndk,* the molecular candidates of the controller and delay mechanism, are predicted to increase the fission frequency since they will reduce the length scale of the system (Fig. 8).

A mechanism based on cellular movements could be tested by altering cell motilities (Endo et al., 2005) or cell lifetime (Pellettieri et al., 2010), while a perturbation on the length of cellular protrusions could test a cellular mechanism via cell contacts, especially by targeting planarian pluripotent stem cells with high protrusions (Zeng et al., 2018). A mechanical realization of the proposed mechanism could be tested by altering the material properties of the connective tissue with RNAi of the collagen and glycoprotein encoding genes found in planaria (Cote et al., 2019). Finally, a bioelectric-based mechanism could be tested by manipulating cellular membrane potentials with ion transport inhibitors (Beane et al., 2011) or gap junction blockers (Emmons-Bell et al., 2015) and observe a difference in fission frequency. In addition, a bioelectrical mechanism could be tested with a membrane voltage reporter assay (Beane et al., 2011; Beane et al., 2013) and observe an intercalated de-hyper-de-hyperpolarized voltage pattern before fission occurs. However, these perturbations to elucidate the physical realization of the model can have pleiotropic effects on other components, and hence control measurements need to be done to ensure that there are no indirect perturbances. As an alternative, the dynamics of cellular movements recorded *in vivo* (Tasaki et al., 2016) during planarian fission can be analyzed to infer a particular cellular interaction function with respect distance, which would be different for a molecular, cellular, or mechanical realization of the cross-inhibited Turing system (Hiscock and Megason, 2015).

The proposed model predicts ectopic tail and head signals, which may trigger the development of tail and head early morphological structures anteriorly and posteriorly, respectively, to the plane of fission. The brain is the most striking organ in the head, and hence the repatterning posterior to the fission plane may show evidence of cephalic ganglia formation as a precursor of the new brain. The rearrangement of these neural structures before fission may be tested at the bench with molecular neural markers (Ross et al., 2017) or with connectivity visualizations with injectable markers (Lerner et al., 2016). In addition, transplanting trunk and head pieces to an intact worm can produce ectopic head and tail structures (Rojo-Laguna et al., 2019; Kobayashi et al., 1999), an approach that could be used to experimentally produce sequential ectopic tail and head structures, which the model predicts to induce fission.

In summary, planarians represent an extraordinary organism to test the patterning mechanisms predicted by Turing systems in growing domains and its molecular, cellular, mechanical, or bioelectrical implementation, which will pave the way for the understanding of the signals governing morphogenesis and regeneration.

10. Methods

PDE simulations were performed in a growing one-dimensional regular grid, where at a constant interval the domain was extended by a new grid cell and the morphogen expression levels linearly interpolated to the new domain size. All simulations started with a stable initial condition similar to a wild-type intact worm as shown in the figures: the head activator and inhibitor with a single peak in the anterior end of the domain, the tail activator and inhibitor with a single peak in the posterior end of the domain, and, when applicable, the controller and delay products with a single peak in the anterior end of the domain. The system was numerically solved with a generalized Runge-Kutta fourth-order solver using ROWMAP (Weiner et al., 1997). Simulation computations used MATLAB R2017b (The MathWorks, Inc.). Stability analysis used an analytical solver to calculate the roots of the system, Jacobian, and eigenvalues, and a numerical evaluation (as in (Smith and Dalchau, 2018)) for the dispersion relation. Analysis computations used Mathematica 11.3 (Wolfram Research, Inc.).

Acknowledgments

We thank Tagide deCarvalho, Julie Wolf, Fernando Vonhoff, the members of the Lobo Lab, and the planarian regeneration community for helpful discussions. This work was supported by the National Science Foundation (NSF) under grant IIS-1566077 and the UBM program at UMBC under NSF grant DBI-1031420. Computations used the UMBC High Performance Computing Facility (HPCF) supported by the NSF MRI program grants OAC-1726023, CNS-0821258, and CNS-1228778, the SCREMS program grant DMS-0821311, and UMBC.

References

Arnold, C.P., Benham-Pyle, B.W., Lange, J.J., Wood, C.J., Sánchez Alvarado, A, 2019. Wnt and TGFβ coordinate growth and patterning to regulate size-dependent behaviour. Nature doi:10.1038/s41586-019-1478-7.

Baker, R.E., Gaffney, E.A., Maini, P.K, 2008. Partial differential equations for self-organization in cellular and developmental biology. Nonlinearity 21, R251–R290. doi:10.1088/0951-7715/21/11/R05.

Beane, W.S., Morokuma, J., Adams, D.S., Levin, M, 2011. A chemical genetics approach reveals H,K-ATPase-mediated membrane voltage is required for planarian head regeneration. Chem. Biol. 18, 77–89.

Beane, W.S., Morokuma, J., Lemire, J.M., Levin, M, 2013. Bioelectric signaling regulates head and organ size during planarian regeneration. Development 140, 313–322. doi:10.1242/dev.086900.

Bely, a.E., Wray, G.a., 2001. Evolution of regeneration and fission in annelids: insights from engrailed- and orthodenticle-class gene expression. Development 128, 2781–2791 doi:11526083.

Best, J.B., Abelein, M., Kreutzer, E., Pigon, A, 1975. Cephalic mechanism for social control of fissioning in planarians: III. Central nervous system centers of facilitation and inhibition. J. Comp. Physiol. Psychol. 89, 923–932. doi:10.1037/h0077164.

Best, J.B., Goodman, A.B., Pigon, A, 1969. Fissioning in Planarians: control by the brain. Science 164, 565–566. doi:10.1126/science.164.3879.565.

Best, J.B., Howell, W., Riegel, V., Abelein, M, 1974. Cephalic mechanism for social control of fissioning in planarians: i. Feedback cue and switching characteristics. J. Neurobiol. 5, 421–442. doi:10.1002/neu.480050505.

Brinkmann, F., Mercker, M., Richter, T., Marciniak-Czochra, A, 2018. Post-Turing tissue pattern formation: advent of mechanochemistry. PLOS Comput. Biol. 14, e1006259. doi:10.1371/journal.pcbi.1006259.

Brøndsted, H.V., 1969. Planarian Regeneration. Pergamon Press.

Bueno, D., Fernàndez-Rodríguez, J., Cardona, A., Hernàndez-Hernà;ndez, V., Romero, R, 2002. A novel invertebrate trophic factor related to invertebrate neurotrophins is involved in planarian body regional survival and asexual reproduction. Dev. Biol. 252, 188–201. doi:10.1006/dbio.2002.0851.

Cebrià, F., Adell, T., Saló, E, 2018. Rebuilding a planarian: from early signaling to final shape. Int. J. Dev. Biol. 62, 537–550. doi:10.1387/ijdb.180042es.

Cebrià, F., Kobayashi, C., Umesono, Y., Nakazawa, M., Mineta, K., Ikeo, K., et al., 2002. FGFR-related gene nou-darake restricts brain tissues to the head region of planarians. Nature 419, 620–624. doi:10.1038/nature01042, 2002/10/11.

Child, C.M., 1910. Physiological isolation of parts and fission in planaria. Arch für Entwicklungsmechanik der Org. 30, 159–205. doi:10.1007/BF02263808.

Child, C.M., 1911. Studies on the dynamics of morphogenesis and inheritance in experimental reproduction. III. The formation of new zoöids in Planaria and other forms. J. Exp. Zool. 11, 221–280. doi:10.1002/jez.1400110303.

Cohen, M., Georgiou, M., Stevenson, N.L., Miodownik, M., Baum, B, 2010. Dynamic filopodia transmit intermittent delta-notch signaling to drive pattern refinement during lateral inhibition. Dev. Cell. 19, 78–89. doi:10.1016/j.devcel.2010.06.006, Elsevier Ltd.

Cote, L.E., Simental, E., Reddien, P.W, 2019. Muscle functions as a connective tissue and source of extracellular matrix in planarians. Nat. Commun. 10, 1592. doi:10.1038/s41467-019-09539-6, Springer US.

Crampin, E.J., Gaffney, E.A., Maini, P.K, 2002. Mode-doubling and tripling in reaction-diffusion patterns on growing domains: a piecewise linear model. J. Math. Biol. 44, 107–128. doi:10.1007/s002850100112.

Crampin, E.J., Gaffney, E.a., Maini, P.K., 1999. Reaction and diffusion on growing domains: scenarios for robust pattern formation. Bull. Math. Biol. 61, 1093–1120. doi:10.1006/bulm.1999.0131.

Crampin, E.J., Hackborn, W.W., Maini, P.K, 2002. Pattern formation in reaction-diffusion models with nonuniform domain growth. Bull. Math. Biol. 64, 747–769. doi:10.1006/bulm.2002.0295.

Durant, F., Lobo, D., Hammelman, J., Levin, M, 2016. Physiological controls of large-scale patterning in planarian regeneration: a molecular and computational perspective on growth and form. Regeneration 3, 78–102. doi:10.1002/reg2.54.

Economou, A.D., Ohazama, A., Porntaveetus, T., Sharpe, P.T., Kondo, S., Basson, M.A., et al., 2012. Periodic stripe formation by a Turing mechanism operating at growth zones in the mammalian palate. Nat. Genet. 44, 348–351. doi:10.1038/ng.1090, 2012/02/22.

Emmons-Bell, M., Durant, F., Hammelman, J., Bessonov, N., Volpert, V., Morokuma, J., et al., 2015. Gap junctional blockade stochastically induces different species-specific head anatomies in genetically wild-type girardia dorotocephala flatworms. Int. J. Mol. Sci. 16, 27865–27896. doi:10.3390/ijms161126065.

Endo, Y., Wolf, V., Muraiso, K., Kamijo, K., Soon, L., Üren, A., et al., 2005. Wnt-3a-dependent cell motility involves RhoA activation and is specifically regulated by dishevelled-2. J. Biol. Chem. 280, 777–786. doi:10.1074/jbc.M406391200.

Forsthoefel, D.J., Newmark, P.A., 2009. Emerging patterns in planarian regeneration. Curr. Opin. Genet. Dev. 19, 412–420. doi:10.1016/j.gde.2009.05.003.

Gierer, A., Meinhardt, H., 1972. A theory of biological pattern formation. Kybernetik 12, 30–39.

Glover, J.D., Wells, K.L., Matthäus, F., Painter, K.J., Ho, W., Riddell, J., et al., 2017. Hierarchical patterning modes orchestrate hair follicle morphogenesis. PLoS Biol. doi:10.1371/journal.pbio.2002117.

Gurley, K.A., Elliott, S.A., Simakov, O., Schmidt, H.A., Holstein, T.W., Alvarado, A.S., et al., 2010. Expression of secreted Wnt pathway components reveals unexpected complexity of the planarian amputation response. Dev. Biol. 347, 24–39. doi:10.1016/j.ydbio.2010.08.007, 2010/08/17Elsevier Inc;.

Gurley, K.A., Rink, J.C., Sánchez Alvarado, A., Alvarado, A.S, 2008. β-Catenin defines head versus tail identity during planarian regeneration and homeostasis. Science 319, 323–327. doi:10.1126/science.1150029.

Handberg-Thorsager, M., Saló, E., 2007. The planarian nanos-like gene Smednos is expressed in germline and eye precursor cells during development and regeneration. Dev. Genes Evol. 217, 403–411. doi:10.1007/s00427-007-0146-3.

Hiscock, T.W., Megason, S.G., 2015. Mathematically guided approaches to distinguish models of periodic patterning. Development 142, 409–419. doi:10.1242/dev.107441.

Hori, I., Kishida, Y., 1998. A fine structural study of regeneration after fission in the planarian Dugesia japonica. Hydrobiologia 383, 131–136. doi:10.1023/A:100341510.

Iglesias, M., Gomez-Skarmeta, J.L., Saló, E., Adell, T, 2008. Silencing of Smed-βcatenin1 generates radial-like hypercephalized planarians. Development 135, 1215–1221.

Kobayashi, C., Nogi, T., Watanabe, K., Agata, K, 1999. Ectopic pharynxes arise by regional reorganization after anterior/posterior chimera in planarians. Mech. Dev. 89, 25–34. doi:10.1016/S0925-4773(99)00192-6.

Kondo, S., Asai, R., 1995. A reaction-diffusion wave on the skin of the marine angelfish Pomacanthus. Nature 765–768. doi:10.1038/376765a0.

Kulesa, P.M., Cruywagen, G.C., Lubkin, S.R., Maini, P.K., Sneyd, J., Ferguson, M.W.J., et al., 1996. On a model mechanism for the spatial patterning of teeth primordia in the alligator. J. Theor. Biol. 180, 287–296. doi:10.1006/jtbi.1996.0103.

Lander, R., Petersen, C.P., 2016. Wnt, Ptk7, and FGFRL expression gradients control trunk positional identity in planarian regeneration. Elife 5, 1689–1699. doi:10.7554/eLife.12850.

Lerner, T.N., Ye, L., Deisseroth, K, 2016. Communication in neural circuits: tools, opportunities, and challenges. Cell 164, 1136–1150. doi:10.1016/j.cell.2016.02.027.

Livshits, A., Shani-Zerbib, L., Maroudas-Sacks, Y., Braun, E., Keren, K, 2017. Structural inheritance of the actin cytoskeletal organization determines the body axis in regenerating hydra. Cell Rep. ElsevierCompany 18, 1410–1421. doi:10.1016/j.celrep.2017.01.036.

Lobo, D., Beane, W.S., Levin, M, 2012. Modeling planarian regeneration: a primer for reverse-engineering the worm. PLoS Comput. Biol. 8, e1002481. doi:10.1371/journal.pcbi.1002481.

Lobo, D., Levin, M., 2015. Inferring regulatory networks from experimental morphological phenotypes: a computational method reverse-engineers planarian regeneration. PLoS Comput. Biol. 11, e1004295. doi:10.1371/journal.pcbi.1004295.

Lobo, D., Levin, M., 2017. Computing a worm: reverse-engineering planarian regeneration. In: Adamatzky, A. (Ed.), Advances in Unconventional Computing Volume 2: Prototypes, Models and Algorithms. Springer International Publishing, pp. 637–654. doi:10.1007/978-3-319-33921-4_24.

Lobo, D., Malone, T.J., Levin, M, 2013. Towards a bioinformatics of patterning: a computational approach to understanding regulative morphogenesis. Biol. Open 2, 156–169. doi:10.1242/bio.20123400.

Lobo, D., Malone, T.J., Levin, M, 2013. Planform: an application and database of graph-encoded planarian regenerative experiments. Bioinformatics 29, 1098–1100. doi:10.1093/bioinformatics/btt088.
Lobo, D., Morokuma, J., Levin, M, 2016. Computational discovery and in vivo validation of hnf4 as a regulatory gene in planarian regeneration. Bioinformatics 32, 2681–2685. doi:10.1093/bioinformatics/btw299.
Lobo, D., Solano, M., Bubenik, G.A., Levin, M, 2014. A linear-encoding model explains the variability of the target morphology in regeneration. J. R. Soc. Interface 11. doi:10.1098/rsif.2013.0918.
Malinowski, P.T., Cochet-Escartin, O., Kaj, K.J., Ronan, E., Groisman, A., Diamond, P.H., et al., 2017. Mechanics dictate where and how freshwater planarians fission. PNAS 114, 201700762. doi:10.1073/pnas.1700762114.
Marcon, L., Sharpe, J., 2012. Turing patterns in development: what about the horse part? Curr. Opin. Genet. Dev. 22, 578–584. doi:10.1016/j.gde.2012.11.013.
Meinhardt, H., 1982. Models of Biological Pattern Formation. Academic Press.
Meinhardt, H., 1993. A model for pattern formation of hypostome, tentacles, and foot in hydra: how to form structures close to each other, how to form them at a distance. Dev. Biol. 157, 321–333.
Meinhardt, H., 2009. Models for the generation and interpretation of gradients. Cold Spring Harb. Perspect. Biol. 1. doi:10.1101/cshperspect.a001362.
Meinhardt, H., Gierer, A., 1974. Applications of a theory of biological pattern formation based on lateral inhibition. J. Cell Sci. 15, 321–346.
Mercker, M., Hartmann, D., Marciniak-Czochra, A, 2013. A mechanochemical model for embryonic pattern formation: coupling tissue mechanics and morphogen expression. PLoS One 8, 1–6. doi:10.1371/journal.pone.0082617.
Mercker, M., Köthe, A., Marciniak-Czochra, A, 2015. Mechanochemical symmetry breaking in hydra aggregates. Biophys. J. 108, 2396–2407. doi:10.1016/j.bpj.2015.03.033.
Miura, T., Shiota, K., Morriss-Kay, G., Maini, P.K, 2006. Mixed-mode pattern in Doublefoot mutant mouse limb-Turing reaction-diffusion model on a growing domain during limb development. J. Theor. Biol. 240, 562–573. doi:10.1016/j.jtbi.2005.10.016.
Morita, M., Best, J.B., 1984. Effects of photoperiods and melatonin on planarian asexual reproduction. J. Exp. Zool. 231, 273–282.
Moustakas-Verho, J.E., Zimm, R., Cebra-Thomas, J., Lempiäinen, N.K., Kallonen, A., Mitchell, K.L., et al., 2014. The origin and loss of periodic patterning in the turtle shell. Development 141, 3033–3039. doi:10.1242/dev.109041.
Murray, J.D, 2003. Mathematical Biology II - Spatial Models and Biomedical Applications, 3rd ed Interdisciplinary applied mathematics. Springer doi:10.1007/b98869.
Myohara, M., Yoshida-Noro, C., Kobari, F., Tochinai, S, 1999. Fragmenting oligochaete Enchytraeus japonensis: A new material for regeneration study. Dev. Growth Differ. 41, 549–555. doi:10.1046/j.1440-169x.1999.00455.x.
Nakamasu, A., Takahashi, G., Kanbe, A., Kondo, S, 2009. Interactions between zebrafish pigment cells responsible for the generation of Turing patterns. Proc. Natl. Acad. Sci. 106, 8429–8434. doi:10.1073/pnas.0808622106.
Newmark, P., Alvarado, A, 2002. Not your father's planarian: a classic model enters the era of functional genomics. Nat. Rev. Genet. 3, 210–219.
Pellettieri, J., Fitzgerald, P., Watanabe, S., Mancuso, J., Green, D.R., Sánchez Alvarado, A., et al., 2010. Cell death and tissue remodeling in planarian regeneration. Dev. Biol. 338, 76–85. doi:10.1016/j.ydbio.2009.09.015, 2009/09/22. Elsevier Inc.
Petersen, C.P., Reddien, P.W., 2008. Smed-βcatenin-1 is required for anteroposterior blastema polarity in planarian regeneration. Science 319, 327–330.
Pietak, A., Levin, M., 2017. Bioelectric gene and reaction networks: computational modelling of genetic, biochemical and bioelectrical dynamics in pattern regulation. J. R. Soc. Interface 14, 20170425. doi:10.1098/rsif.2017.0425.
Pigon, A., Morita, M., Best, J.B, 1974. Cephalic mechanism for social control of fissioning in planarians: II. Localization and identification of the receptors by electron micrographic and ablation studies. J. Neurobiol. 5, 443–462. doi:10.1002/neu.480050506.
Quinodoz, S., Thomas, M.A., Dunkel, J., Schötz, E.M, 2011. The more the Merrier?: Entropy and statistics of asexual reproduction in freshwater planarians. J. Stat. Phys. 142, 1324–1336. doi:10.1007/s10955-011-0157-3.
Raspopovic, J., Marcon, L., Russo, L., Sharpe, J, 2014. Digit patterning is controlled by a Bmp-Sox9-Wnt Turing network modulated by morphogen gradients. Science 345, 566–570. doi:10.1126/science.1252960.
Reddien, P.W., 2018. The cellular and molecular basis for planarian regeneration. Cell 175, 327–345. doi:10.1016/j.cell.2018.09.021, Elsevier Inc.
Reddien, P.W., Sánchez Alvarado, A, 2004. Fundamentals of planarian regeneration. Annu. Rev. Cell Dev. Biol. 20, 725–757.
Rojo-Laguna, J.I., Garcia-Cabot, S., Saló, E, 2019. Tissue transplantation in planarians: a useful tool for molecular analysis of pattern formation. Semin. Cell Dev. Biol. 87, 116–124. doi:10.1016/j.semcdb.2018.05.022, Elsevier Ltd.
Ross, K.G., Currie, K.W., Pearson, B.J., Zayas, R.M, 2017. Nervous system development and regeneration in freshwater planarians. Wiley Interdiscip. Rev. Dev. Biol. 6, 1–26. doi:10.1002/wdev.266.
Sakurai, T., Lee, H., Kashima, M., Saito, Y., Hayashi, T., Kudome-Takamatsu, T., et al., 2012. The planarian P2X homolog in the regulation of asexual reproduction. Int. J. Dev. Biol. 56, 173–182. doi:10.1387/ijdb.113439ts, 2012/03/28.
Schiffmann, Y., 2011. Turing-child field underlies spatial periodicity in Drosophila and planarians. Prog. Biophys. Mol. Biol. 105, 258–269.
Scimone, M.L., Cote, L.E., Rogers, T., Reddien, P.W, 2016. Two FGFRL-Wnt circuits organize the planarian anteroposterior axis. Elife 5, 1–19. doi:10.7554/eLife.12845.
Sharpe, J., 2017. Computer modeling in developmental biology: growing today, essential tomorrow. Development 144, 4214–4225. doi:10.1242/dev.151274.
Sheĭman, I.M., Sakharova, N.I., Tiras, K.P., Shkutin, M.F., Isaeva, V.V., 2003. Regulation of asexual reproduction in the planarian Dugesia tigrina. Russ. J. Dev. Biol. 34, 36–41. doi:10.1023/A:1022237817666.
Smith, S., Dalchau, N., 2018. Model reduction enables Turing instability analysis of large reaction–diffusion models. J. R. Soc. Interface 15, 20170805. doi:10.1098/rsif.2017.0805.
Stückemann, T., Cleland, J.P., Werner, S., Thi-Kim Vu, H., Bayersdorf, R., Liu, S.-Y., et al., 2017. Antagonistic self-organizing patterning systems control maintenance and regeneration of the anteroposterior axis in planarians. Dev. Cell 40, 248–263. doi:10.1016/j.devcel.2016.12.024, e4.
Sureda-Gómez, M., Martín-Durán, J.M., Adell, T, 2016. Localization of planarian β-CATENIN-1 reveals multiple roles during anterior-posterior regeneration and organogenesis. Development 143, 4149–4160. doi:10.1242/dev.135152.
Tasaki J., Uchiyama-Tasaki C., Rouhana L. Analysis of stem cell motility in vivo based on immunodetection of planarian neoblasts and tracing of BrdU-labeled cells after partial irradiation. 2016. pp. 323–338. doi:10.1007/978-1-4939-3124-8_18
Thomas, M.A., Quinodoz, S., Schötz, E.M, 2012. Size matters!: birth size and a size-independent stochastic term determine asexual reproduction dynamics in freshwater planarians. J. Stat. Phys. 148, 663–675. doi:10.1007/s10955-012-0514-x.
Turing, A.M., 1952. The chemical basis of morphogenesis. Philos. Trans. R. Soc. Lond. B Biol. Sci. 237, 37–72.
Umesono, Y., 2018. Postembryonic axis formation in planarians. In: Kobayashi, K., Kitano, T., Iwao, Y., K, M. (Eds.), Reproductive and Developmental Strategies Diversity and Commonality in Animals. Springer, Japan, pp. 743–761. doi:10.1007/978-4-431-56609-0_33.
Umesono, Y., Tasaki, J., Nishimura, Y., Hrouda, M., Kawaguchi, E., Yazawa, S., et al., 2013. The molecular logic for planarian regeneration along the anterior-posterior axis. Nature 500, 73–76. doi:10.1038/nature12359, Nature Publishing Group.
Vandel, A, 1922. Recherches expérimentales sur les modes de reproduction des planaires triclades paludicoles. Universite de Paris.
Walton, K.D., Whidden, M., Kolterud, A., Shoffner, S., Czerwinski, M.J., Kushwaha, J., et al., 2015. Villification in the mouse: Bmp signals control intestinal villus patterning. Development 734–764. doi:10.1242/dev.130112.
Weiner, R., Schmitt, B.A., Podhaisky, H, 1997. ROWMAP–a ROW-code with Krylov techniques for large stiff ODEs. Appl. Numer. Math. 25, 303–319. doi:10.1016/S0168-9274(97)00067-6.
Werner, S., Stückemann, T., Beirán Amigo, M., Rink, J.C., Jülicher, F., Friedrich, B.M., et al., 2015. Scaling and regeneration of self-organized patterns. Phys. Rev. Lett. 114, 138101. doi:10.1103/PhysRevLett.114.138101.
Woolley, T.E., Baker, R.E., Gaffney, E.A., Maini, P.K, 2011. Stochastic reaction and diffusion on growing domains: understanding the breakdown of robust pattern formation. Phys. Rev. E - Stat. Nonlin. Soft Matter Phys. 84, 1–16. doi:10.1103/PhysRevE.84.046216.
Yang, X., Kaj, K.J., Schwab, D.J., Collins, E.-M.S, 2017. Coordination of size-control, reproduction and generational memory in freshwater planarians. Phys. Biol. 14, 036003. doi:10.1088/1478-3975/aa70c4.
Zeng, A., Li, H., Guo, L., Gao, X., McKinney, S., Wang, Y., et al., 2018. Prospectively isolated tetraspanin+neoblasts are adult pluripotent stem cells underlying planaria regeneration. Cell 173, 1593–1608. doi:10.1016/j.cell.2018.05.006, e20.